Post-print

Full version available at: doi: 10.1038/ncomms8627

24 # Persistent drying in the tropics linked to natural forcing

25

26 Amos Winter[1], Davide Zanchettin[2,3], Thomas Miller[1], Yochanan Kushnir[4], David Black[5],
27 Gerrit Lohmann[6], Allison Burnett[7], Gerald Haug[8], Juan Estrella-Martínez[1], Sebastian
28 F.M. Breitenbach[9,10], Luc Beaufort[11], Angelo Rubino[3], Hai Cheng[7,12]

29

30 1. University of Puerto Rico, Mayagüez, Puerto Rico 00681-9000, USA
31 2. Max Planck InstituteforMeteorology, Bundesstr. 53, 20157 Hamburg, Germany
32 3. University of Venice, Dorsoduro 2137, 30123 Venice, Italy
33 4. Lamont-Doherty Earth Observatory of Columbia University, Palisades, New York 10964, USA
34 5. Stony Brook University, Stony Brook, New York 11790, USA
35 6. Alfred Wegener Institute, Helmholtz Centre for Polar and Marine Research,
36 27570Bremerhaven,Germany
37 7. University of Minnesota, Minneapolis, Minnesota 55455, USA
38 8. Swiss Federal Institute of Technology, Zurich 8092, Switzerland.
39 9. Department of Earth Sciences, University of Cambridge, Downing Street, Cambridge CB2 3EQ, UK
40 10. Sediment and Isotope Geology, Ruhr-University Bochum, Universitätsstr. 150, 44801, Bochum,
41 Germany
42 11. CEREGE (CNRS-Université Aix Marseille), 13545 Aix en Provence, France
43 12. Xi'an Jiaotong University, Xi'an 710049, China

44

45 **Approximately half the world's population lives in the tropics, and future changes in**

46 **the hydrological cycle will impact not just freshwater supplies, but also energy**

47 **production in areas dependent upon hydroelectric power. It is vital that we understand**

48 **the mechanisms/processes that affect tropical precipitation and the eventual surface**

49 **hydrological response to better assess projected future regional precipitation trends**

50 **and variability. Paleoclimate proxies are well suited for this purpose as they provide**

51 **long time series that pre-date and complement the present, often short instrumental**

52 **observations. Here we present paleo-precipitation data from a speleothem located in**

53 **Mesoamerica that reveal large multi-decadal declines in regional precipitation, whose**

54 **onset coincides with clusters of large volcanic eruptions during the 19th and 20th**

55 **centuries. This reconstruction provides new independent evidence of long-lasting**

56 **volcanic effects on climate and elucidates key aspects of the causal chain of physical**

57 **processes determining the tropical climate response to global radiative forcing.**

58

59 The climate of Mesomerica (Fig. 1a) is characterized by a boreal summer/fall (June-October)

60 rainy season and a relatively dry winter[1]. Mesoamerica's rainfall is influenced by moisture

61 originating usually from the vicinity of the Intertropical Convergence Zone (ITCZ) via

62 transport into the monsoonal system over Belize, via the Caribbean low-level jet, and by

63 localized convection. In summer, the ITCZ migrates to its northern position, its core

64 stretching across the northern tropical Atlantic at ~10°N, into northern South America and

65 from there turning north over Central America to the East Pacific, reaching to ~12°N and

66 causing widespread rainfall over the land portion[2]. Because the two ITCZ segments respond

67 to variations in sea-surface temperatures (SSTs) in both the tropical Atlantic and the Pacific

68 Oceans, Mesoamerica is exposed to complex hydrological fluctuations on a broad range of

69 timescales[3]. Year-to-year rainfall variability in the Guatemala mountain regions today is

70 correlated with the gradient between SSTs in the western tropical Atlantic and eastern

71 tropical Pacific[1]. Colder (Warmer) than normal tropical Atlantic SSTs, which are consistent

72 with a stronger (weaker) and more southward (northward) displaced Atlantic Subtropical

73 High, lead to drier (wetter) than normal conditions in Central America[4,5]. Similarly,

74 anomalously warm (cold) eastern equatorial Pacific SSTs, e.g., during El Niño (La Niña)

75 events, force an equatorward (northward) displacement of the east Pacific ITCZ and

76 contribute to drying (wetting) in most of Central America[6,7]. Observations also indicate an

77 association between precipitation conditions over Mesoamerica and the phasing of the winter

78 North Atlantic Oscillation (NAO)[8].

79   Timing and distribution of precipitation during the summer season is a critical issue for

80   agricultural yields in Yucatán, and periods of drought vitally affect agriculture and, hence,

81   local societies [new ref:]. Observational meteorological records indicate that droughts on the

82   peninsula are much rare and tend to be more severe than wet periods [same ref as above].

83   However, the availability of continuous, long-term hydrological data beyond the few

84   decades covered by the instrumental record is a necessary prerequisite to fully characterize

85   regional hydrological variability and to uncontroversially address its dependence on large-

86   scale climatic fluctuations, especially the identification of forcing mechanisms at the

87   hemispheric to global scales. Speleothems are increasingly used as terrestrial archives of past

88   climate and environmental change because they can provide long, continuous, precisely U-

89   series dated and high-resolution time series, and are generally unaffected by post-

90   depositional diagenetic alteration. Here we present results from a new 300 yr (1700-2000

91   C.E.) $\delta^{18}O$ reconstruction based on a speleothem from Mesoamerica demonstrating, for the

92   first time, that natural external forcing can drive successive multi-decadal dry and wet

93   phases in the tropics.

94

95   **Results**

96   **Hydrological reconstruction and volcanic eruptions.**

97   The data for this study derive from stalagmite GU-Xi-1 collected 250 m inside the large

98   cavern of Xibalba in the Campur Formation[9] located in the Maya Mountains of Guatemala

99   near the Belize border (Fig. 1a, 16.5ºN, 89ºW). The in-cave elevation is 350 m, with a cave

100   mean annual temperature of 23°C. GU-Xi-1 was actively dripping at the time of collection,

101   and chosen for its candle-shape, its distance from outside atmospheric influences, and its

102   location of 30 meters above the nearby modern river level; the karst surface is generally 100-

103   150 m above the cave passages (Fig. 1b). The specimen is 33 centimeters tall, but only the

104   upper 18 centimeters are used for this study (Fig. 2a). Our age model (Fig. 2b) is

105   highlyconstrained by nine U/Thmulticollector inductively coupled plasma mass

106   spectrometry dates (Supplementary Table 1) and by the collection date in 2007.

107   The largest amounts of annual precipitation in the region fall on the high mountain ranges

108   of Guatemala, southwest of the cave. Summer precipitation values in the Maya Mountains

109   reach upwards of 400 mm/month, but are approximately half that amount in the study area. A

110   strong inverse correlation between speleothem $\delta^{18}O$ and tropical precipitation intensity[10] has

111   previously been observed for the region[11]. The speleothem $\delta^{18}O$significantly correlates (see

112   methods) with precipitation from nearby Belize City over the instrumental period, when a lag

113   of six years is imposed to the former (Fig. 3). The inverted correlation patterns of the

114   speleothem $\delta^{18}O$ with the SST and sea-level pressure (SLP) fields over the Pacific and Atlantic

115   sectors is consistent with corresponding patterns for observed precipitation (Fig. 4), supporting

116   the robustness of the climatological scenario associated with interannual rainfall variability

117   over the Yucatán.

118   The most prominent aspects of our reconstruction are the occurrences of three distinct

119   multi-decadal drying trends during the 19th and 20th centuries (Fig. 5e). Based on the modern

120   relationship between $\delta^{18}O$ and regional precipitation anomalies[12], the speleothem data indicate

121   a 25% decrease in precipitation between 1810 and 1845 C. E., another comparable

122   precipitation decrease between 1883 and 1925 C. E., and a third, smaller decrease from 1963 to

123   the present. The drying steps are separated from one another by brief intervals of precipitation

124   recovery in mid-century. Our and other available $\delta^{18}O$ records from Mesoamerica[13,14] correlate

125 with each other with variable strength during the reconstruction period (Fig. 6, Supplementary

126 Figs. 1,2), in part reflecting large dating uncertainties in some of the reconstructions. The

127 different reconstructions feature similar drying trends during the early and – less so – late 19th

128 century, suggesting a broader regional phenomenon.

129 Our three pronounced decreases in regional precipitation coincided with clusters of strong

130 tropical volcanic eruptions (Fig. 5a). The most prominent of these eruptions are the 1809

131 eruption of unknown location and Tambora in 1815 (cluster 1), Krakatau in 1883 (cluster 2),

132 Agung in 1963 and Pinatubo in 1991 (cluster 3). Reconstructed precipitation decreases

133 throughout each cluster such that the precipitation evolution during these periods is best

134 described as a function of cumulative volcanic radiative forcing (Fig. 5b-d, Supplementary

135 Figs. 3,4 and Supplementary Note 1). The different estimates of cumulative volcanic forcing

136 provided in Fig. 5 exemplify the effects of uncertainties such as those in reconstructed aerosol

137 optical properties used as volcanic forcing input to climate models, those arising from the

138 presence of additional varying external forcing factors, and those inherent in the model-

139 specific implementation of volcanic forcing.

140 The most recent volcanic cluster does not display a statistically-significant correlation

141 between $\delta^{18}O$ and cumulative volcanic forcing, that we interpret as the result of the different

142 background climate conditions and of interferences from other dominant forcing factors during

143 the mid- to late-20th century. For the 19th century clusters, the drying trend only reverses when

144 volcanic activity substantially weakens. The precipitation recovery is only partial, possibly as

145 part of recurrent drying trends in Mesoamerica[11,15]. Aerosols are a known critical part of the

146 overall anthropogenic as well as natural forcing of climate (the latter associated with aeolian

147 dust and volcanic eruptions)[16-18]. We thus surmise that the decadal drying trends in the early

148   and late decades of the 19th century and during the second half of the 20th century are largely a

149   consequence of the clustered volcanic forcing, with the most recent period superposed on long-

150   term anthropogenic drying[19,20]. Periods of strong volcanic activity during the last millennium

151   also often coincide with periods of anomalous solar activity. This is the case, for instance, for

152   the first volcanic cluster that coincides with the prolonged period of weak solar activity known

153   as Dalton Minimum[21]. We can thus not attribute the reconstructed changes to volcanic forcing

154   alone.

155

156   **Dynamical interpretation of reconstructed changes**.

157   Based on the close agreement between the drying phases and the volcanic clusters, we

158   hypothesize that the eruption clusters played a primary role in these climatic changes by

159   inducing perturbations in patterns of SST variability that in turn crucially influence the Pacific-

160   Atlantic tropical SST gradient that dominate the Mesoamerican hydroclimate. Specifically, we

161   propose that the volcanic clusters influence the El Niño Southern Oscillation (ENSO) in the

162   equatorial Pacific and the long-term variations of tropical Atlantic SSTs, which is governed by

163   the Atlantic Multidecadal Oscillation (AMO)[22]. An increasing number of climate

164   reconstructions and simulations describe statistical and dynamical connections between

165   volcanic forcing and both ENSO[23] and AMO[24-26]. Indeed, drying (recovery) phases during the

166   volcanic clusters correspond to cold (warm) phases in a recent marine-proxy-based AMO

167   reconstruction[27] (Fig. 7a), while reconstructed data[28] suggest an increased role for ENSO in

168   Mesoamerican precipitation variability during the 20th century (Fig.7b). The preferred time

169   scales of significant coherence with the $\delta^{18}O$ signal differ between ENSO and AMO, as the

170   former index highlights interdecadal time scales (O(30 year)) while the latter highlights multi-

171   decadal time scales (O(50 year)), further suggesting that the linkages may reflect different

172   teleconnection mechanisms (see also Fig. 7c). Such differences in the relative roles of climatic

173   modes indicate that internal dynamics play a substantial role in communicating high

174   atmospheric evolution during the different volcanic eruption clustersto the surface. This

175   exemplifies the complexity of a dynamical interpretation, and hence attribution, of the

176   reconstructed changes in Mesoamerican precipitation. Moreover, reconstructions of climate

177   modes often lack robustness due to the inherent uncertainties implicated in reconstructing

178   large-scale features from a limited number of local climate proxies. This has been shown for

179   the NAO[29] that captures a dominant part of the short- and long-term variability of large-scale

180   atmospheric circulation over the North Atlantic, which is a known factor influencing

181   Mesoamerican precipitation (Fig. 4b,d) and is sensitive to volcanic forcing[30,31].

182   A warranted dynamical interpretation based on modeling results is also complicated by the

183   fact that last-millennium simulations from state-of-the-art global climate models do not show a

184   consistent response of Mesoamerican precipitation to strong volcanic activity (Fig. 8), failing

185   to robustly reproduce the patterns reconstructed from our speleothem. The discrepancy

186   between our reconstruction and the simulations can be ascribed to general deficiencies still

187   affecting the simulated representation of key chemical and physical processes related to aerosol

188   forcing, and to the consequent large uncertainties in the simulated climate response to volcanic

189   forcing[21,32]. Further possible explanations are the common model deficiencies concerning

190   regional precipitation variability at the decadal and multi-decadal time scales[33], which are

191   linked to poor and hence less robustly simulated representation of dominant modes of large-

192   scale climate variability and associated teleconnections including ENSO[34]and the AMO[35].

193   Large uncertainties also affect the reconstructed forcing[36]and we have very limited knowledge

194   about the background climate conditions at the time of volcanic eruptions that occurred prior to

195   the last half of the 20[th]century[26].

196

Discussion

198   The prolonged post-eruption drying conditions in Mesoamerica described by our new

199   speleothem-based data provide independent evidence that volcanic effects on tropical

200   climate persist well beyond the duration of the direct radiative imbalance[31]. We suggest that

201   volcanically-induced changes in dominant modes of large-scale, ocean-atmosphere coupled

202   variability is a likely physical mechanism contributing to such persistence. Further studies

203   are needed to clarify the dynamics governing the response. Still, our observation relating

204   clusters of large volcanic eruptions to prolonged decreased Mesoamerican precipitation

205   should expand the emerging discussion fostered by indications from global climate models

206   regarding the strong sensitivity of the world's other monsoons to external forcing[37,38]. Our

207   results, in combination with studies of global stream flows after large volcanic eruptions[39],

208   imply that certain tropical hydroclimates may be highly sensitive to volcanic forcing and,

209   more generally, to large stratospheric aerosols loading[20]. Global climate models have

210   become increasingly important to our physical understanding of such "global forcing to

211   regional response" connections. As discussed however, related uncertainties affecting the

212   simulated representation (or lack thereof) of key processes as well as the reconstructed

213   external forcing that is imposed on paleo-simulations remain considerable. We need to better

214   understand such critical aspects of reconstructed as well as simulated pre-industrial tropical

215   climate evolution in order to increase our confidence in projected future regional

216 precipitation trends and variability and to potentially customize solutions for particular

217 regions.

218

219 **Methods**

220 **Speleothemcharacteristics and analysis**.We collected the GU-Xi-1 stalagmite in 2007 from

221 the Xibalba cave located in a thick forest near the Guatemala/Belize border(Fig. 1b), and

222 mapped its underground location relative to the surface. The ceiling height varies from 10 m to

223 >40 m. The collection site lies well above the level of modern floods, which eliminates

224 inaccuracies in dating due to possible initial detrital ^{230}Th. GU-Xi-1 was active and growing at

225 the time of collection, with a columnar shape indicating it was a product of a single drip

226 source.The stalagmite was cut into two sections and a 1 cm-thick slab was produced from one

227 of the sections.

228

229 **Age model**. 200 mg of powder were collected with a hand-held dental drill from a polished

230 slab section of GU-Xi-1along growth layers for dating. Nine ^{230}Th dates were analyzed in the

231 upper 175 mm resulting in an age control point approximately every 30 years (Fig. 2a). We

232 analyzed three samples for thorium and uranium isotopes separately on a Finnigan-MAT

233 Element outfitted with a double focusing sector-field magnet in reversed Nier-Johnson

234 geometry and a single Mas Com multiplier. We measured combined ionization plus

235 transmission efficiency of 2.5 to 3‰ for uranium and 1.5 to 2‰ for thorium. Dating resolution

236 using the machine was 40 to 80 years. Six more samples were analyzed with a Neptune ICP-

237 MS MC, with a dating resolution of less than 4 years. Further details of instrumental

238 procedures are explained in[40,41]. We obtained these dates with a magnetic sector inductively-

239   coupled plasma mass spectrometer at the University of Minnesota, Isotope Laboratory[42].

240   Chemical separation procedures followed those described in[43].The age model for the

241   speleothem is based on a parabolic curve fit to the ^{230}Th dates and the collection date (Fig. 2b).

242   Error bars are larger for the ages determined with a Finnigan-MAT Element compared to the

243   dating resolution obtained using the Neptune ICP-MS MC (Fig. 2b). We used Analyseries

244   (http://www.lsce.ipsl.fr/logiciels/index.php) to regress the U/Th ages with depth. We found

245   that the upper section of GU-Xi-1 grew according to a second-degree polynomial that was

246   parabolic (r=0.99). We removed any sampling bias with Analyseries using the integration

247   method to provide evenly spaced annual samples. We used the resulting polynomial equation

248   to convert each sample depth to calendar ages from the speleothem, which we used for our age

249   model.

250   Different possible age models have been tested (Supplementary Fig. 5), including StalAge[44],

251   COPRA[45], calcium (Ca) layer counting and the average between StalAge and the Ca count

252   methods (ChronMean).All the tested models agree closely with the timing of the drying event

253   observed from the stable isotope record associated with the Tamboraeruption. The largest

254   uncertainty is the timing of the Krakatau eruption. It should be noted that because GU-Xi-1

255   growth slowed down considerably towards the present (from 1915 to 2007 it grew 2.5 times

256   slower than from 1840 to 1871) any error for the more recent samples in assigning a depth to a

257   U/Th date is exacerbated. StalAge is a routinely usedalgorithm specifically designed for

258   speleothems. It takes into account outliers and age inversions using a Monte-Carlo simulation.

259   In our case, as we do not have outliers nor age inversions, it basically performs a linear

260   interpolation between age points. A similar age model[45] gives near identical results to that of

261   StalAge. Another approach is to count the annual laminations (clearly present in GU-Xi-1). We

262   are confident the laminations are annual because the number of laminations counted are within

263   97% confidence limits of the U/Th dates. The annual layers are tedious to count and also

264   produce subjective counting errors. Another more objective method is to count the number of

265   annual Ca peaks that clearly follow the annual banding. During summer more Ca is

266   incorporated in the speleothems[46]. The results from this method are shown as the Ca counts

267   chronology in Supplementary Fig. 1 and clearly lie to the right (younger) side of the age model

268   especially from 1830 to the present. According to StalAge the "Krakatau" event (as seen in the

269   stable isotopes) occurred in 1864 (about 20 years earlier) but according to the Ca counts the

270   event occurred in 1910 (about 20 years later). StalAge based on U/Th dates may be biased

271   towards recent samples because of the greater uncertainties (5 to 10% of the absolute age[47]) for

272   younger speleothems with low U, thus limiting the possibility to correlate time-series based on

273   speleothems with those based on instruments. A further approach is to take the mean of both

274   the StalAge and the Ca count methods. The mean is shown as the "ChronMean" in

275   Supplementary Fig. 5. The ChronMean model also smoothes any U/Th depth sampling error.

276   The ChronMean is nearly identical to our parabolic fit for stalagmite GU-Xi-1 from 1750

277   onwards giving us confidence in our age chronology and timing of the isotopes events to the

278   volcano chronology. Furthermore, there is supporting evidence that some stalagmites grow in a

279   parabolic fashion. Parabolic growth of speleothems has been previously noted[48] and may be a

280   natural function of conical growth. Finally, the similarity of our record withthat from another

281   stalagmite from MesoAmerica[13] (Fig. 6) increases our confidence on the robustness of our age

282   model.

283

Samples and δ¹⁸O isotopic analysis. 582 samples were continuously milled along the

stalagmite growth axis of GU-Xi-1 stalagmite using a digitally controlled micro-milling

machine (SHERLINE 5410). Samples were milled at 0.3 mm intervals (Fig. 2a) giving a

temporal resolution ranging between yearly at the top to seasonal at the bottom. Growth rate of

the speleothem fluctuated from approximately 1 to 3 mm per year. The samples were analyzed

using a continuous flow isotope ratio mass spectrometry (CF-IRMS[49])at the ETH Zurich,

Switzerland. Details on the methodology are given in[49]. MS2 was used as in-house reference

material (powdered Carrara marble, MS2[49]), with isotope ratios ($^{18}O/^{16}O$ and $^{13}C/^{12}C$) reported

in standard Delta notation relative to the Vienna Pee Dee Belemnite (‰ VPDB) standard (see

supplementary data 1). The external analytical precision for $\delta^{18}O$ is better than 0.06‰.

Amount Effect. The amount effect on stalagmites has been rigorously studied for Mesoamerica

and has shown to be valid[11,12]. The comparison between precipitation and $\delta^{18}O$ in Fig. 3

indicates that the speleothem's oxygen isotopic properties capture the low-frequency variations

of rainfall outside the cave, with the proportion of heavy isotope inversely proportional to the

amount of precipitation.

Observational datasets. The precipitation data are from the University of East Anglia (UEA) -

Climate Research Unit (CRU) gridded historical Time Series (TS) version 3.21 for 1901 to

2012 (for more information,

see:http://badc.nerc.ac.uk/view/badc.nerc.ac.uk__ATOM__ACTIVITY_0c08abfc-f2d5-11e2-

a948-00163e251233). The SST data are from the NOAA National Climate Data Center

Extended Reconstructed Sea Surface Temperature (ERSST) analysis[50] version 3b averaged

over the summer months between 1901 and 2012 in Fig. 4a, and between1880 and 2006 in Fig.

308   4c to fit with the length of the observed precipitation and $\delta^{18}O$ records, respectively. The SLP

309   data are from the NOAA Environmental Research Laboratories Twentieth Century Reanalysis

310   Project (TCRP)[51] version 2, covering the period between 1901 and 2006 in Fig. 4b and

311   between 1880 and 2006 in Fig. 4d. The SLP data were averaged over the winter (December-

312   March) preceding the summer, as this is when the atmosphere forces the SST pattern seen in

313   Fig. 4a[8]. Support for the TCRP dataset was provided by the U.S. Department of Energy, Office

314   of Science Innovative and Novel Computational Impact on Theory and Experiment (DOE

315   INCITE) program, and Office of Biological and Environmental Research (BER), and by the

316   National Oceanic and Atmospheric Administration Climate Program Office.

317   Data for Belize-City precipitation is from the National Oceanic and Atmospheric

318   Administration, monthly Global Historical Climatology Network (GHCN:

319   http://www.ncdc.noaa.gov/ghcnm/).

320

321   **Simulated precipitation datasets.** Time series of Yucatán precipitation covering the period

322   1700-2005 were obtained from an ensemble of climate model simulations from the repository

323   of the Coupled Model Intercomparison Project 5 (CMIP5). For each model, the time series

324   were created by merging the data from the last-millennium simulation (past1000, which ends

325   in 1849) with the corresponding data from one of the historical simulations (starting in 1850).

326   Yucatán is defined as the area between 91°W and 87°W and between 16°N and 22°N (all

327   model data were interpolated to a 2°x2° grid before selecting the region).

328

329   **Volcanic forcing estimates.** Forcing estimates from ECHAM5/MPIOM[52] and Bergen Climate

330   Model (BCM)[24] are derived from volcanic forcing-only and natural(volcanic and solar) last-

331   millennium simulations. Forcing estimates for CCSM4[53] are derived from the full-forcing last-

332   millennium simulation available in the CMIP5 repository. Long-term influences from

333   greenhouse gases in CCSM4 are accounted for by removing the fourth-order polynomial trend

334   over the period 1750-2005. Natural forcing was then estimated based on clear-sky top-of-

335   atmosphere radiative fluxes to discard cloud related feedbacks. The simulations use different

336   reconstructions of aerosol optical properties for volcanic forcing: ECHAM5/MPIOM uses the

337   reconstruction by[54]; BCM uses the reconstruction by[55]; CCSM4 uses the reconstruction

338   by[56].Cumulative volcanic forcing is obtained by cumulatively adding the forcing of each

339   volcanic event through time.

340

341   **Statistical significance.** Statistical significance for correlations accounts for the effective

342   degrees of freedom based on autocorrelation following the method by[57]. The lag in Fig. 3 was

343   determined based on a cross-correlation analysis between the two time series with lags varying

344   between -10 and +10 years. The binomial smoothed 71-year precipitation record shown in Fig.

345   3 has 15 degrees of freedom, so that a correlation value of 0.43 is significant at the 95% level

346   using a directional test (appropriate in this case as we can surmise that the precipitation is the

347   driver of the $\delta^{18}O$ variations and not vice versa).

348

349   **Wavelet analysis.**Wavelet coherence spectra were calculated using the tool by[58]. For

350   additional information, see:[59]. The power of the wavelet coherence spectrum can be interpreted

351   as a measure of the strength of the local (in the time-frequency domain) correlation between
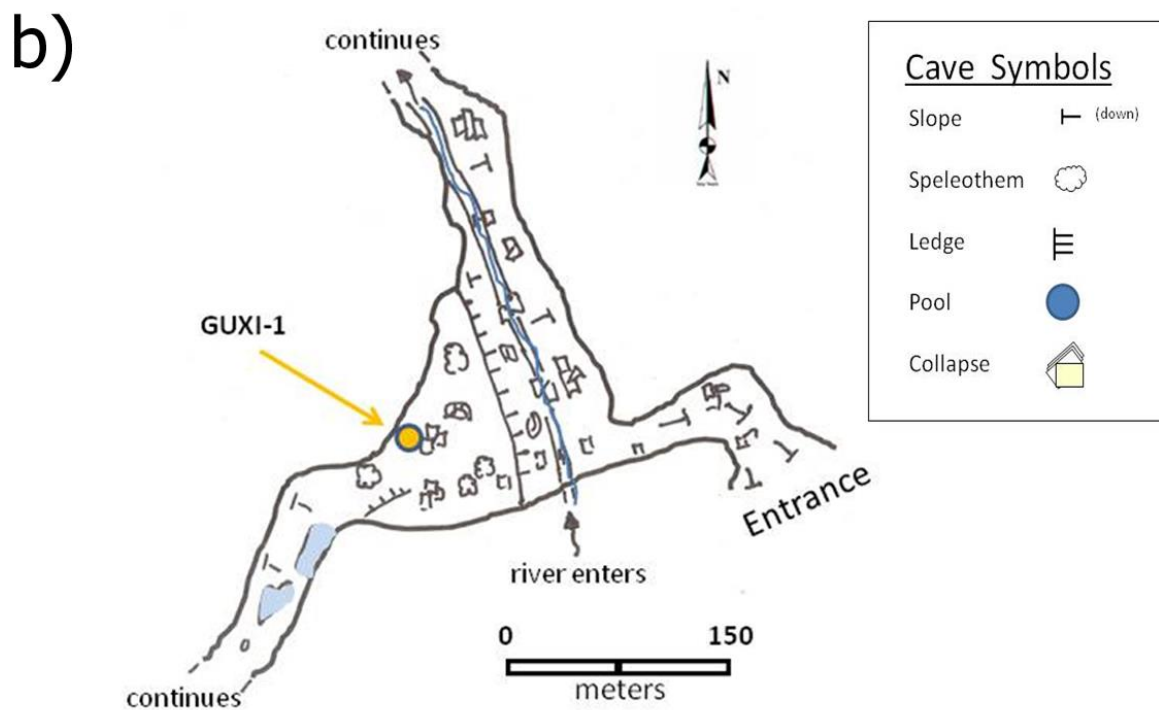
352   the two time series.

353

371 **Author contributions** AW, YK, and DB conceived the project. TM selected and retrieved

372 the stalagmite, and mapped its locations with respect to the surface. AW, DZ, YK, DB, GL

373 and AR wrote most of the paper. AB, GH, JEM, SB, LB, DZ and HC performed the

374 experiments and analytical work.
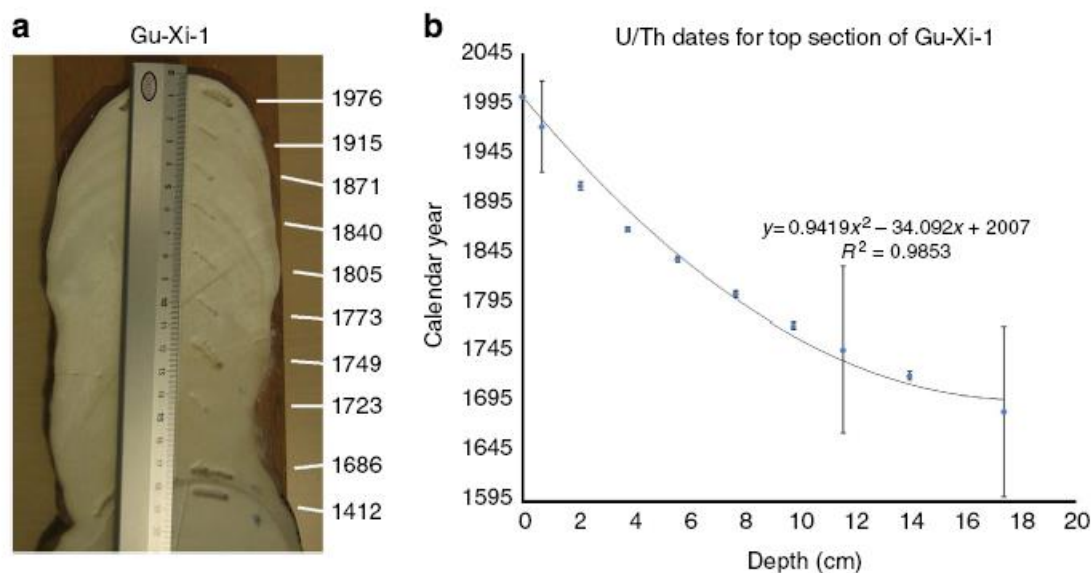
375

376 **Figure Captions**

377

378 **Figure 1: Geographicalcharacteristics of the study area.**(**a**) Location map of Mesoamerica

379 and of the Xibalba cave; (**b**) Map of the speleothem site with major physical features of the

380 cave.

Figure 2: Image of the speleothem andage model. (**a**) The photograph of GU-Xi-1 stalagmite shows the height of the specimen used in this study (18 cm), with a rounded top and no "cup" that could imply drip erosion. Also shown is the milling channel for the stable isotopes adjacent to a cm ruler as well as the nine pits on stalagmite GU-Xi-1 used to determine 230Th. (**b**) Age model.
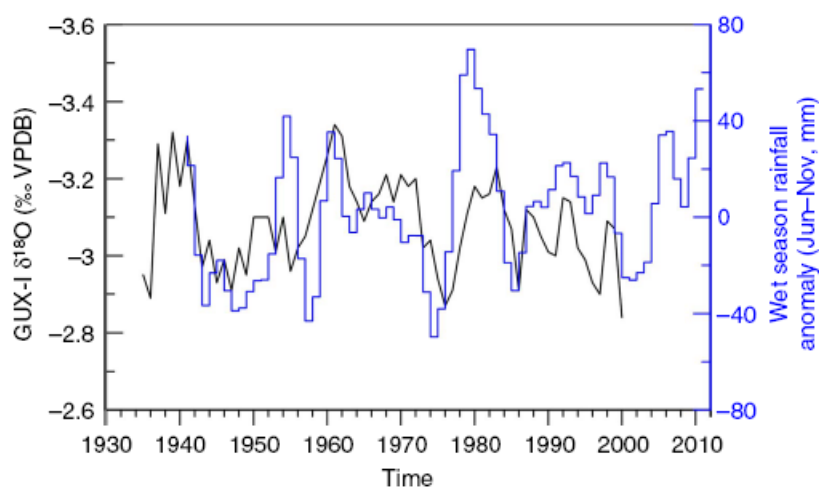

Figure 3: Comparison between reconstructed and observed Mesoamerican precipitation. Shown are the time series of speleothem GU-Xi-1 $\delta^{18}O$ (black line, units in permil) and June to November precipitation anomalies in Belize City, Belize (deviation from climatology in mm,

393 blue line) smoothed with a second order binomial filter. The δ^{18}O time series lags the rainfall

394 time series by six years.

395
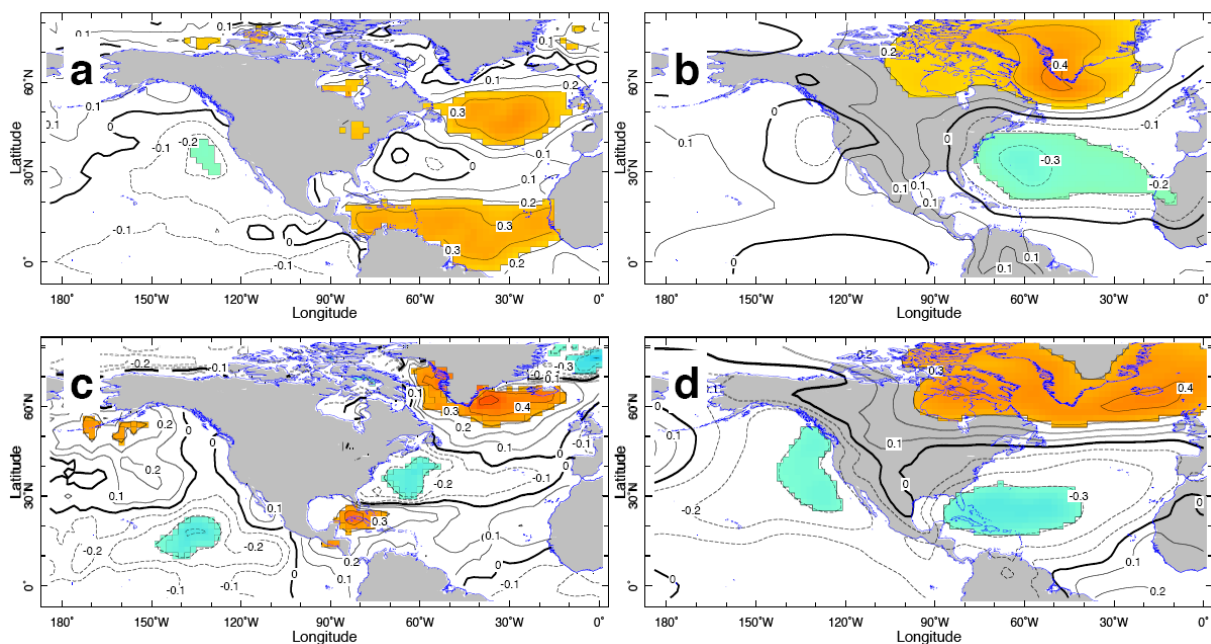
396

397 **Figure 4: Atmosphere and ocean relationships to Mesoamerican rainfall.** (**a**, **b**)

398 Correlations between summertime (May-October) observed precipitation averaged over the

399 Yucatán Peninsula and sea-surface temperature (SST, **a**) and sea level pressure (SLP,**b**). (**c**, **d**)

400 Correlations of the SST and SLP fields with the GU-Xi-1 speleothemδ^{18}O (multiplied by -1).

401 Contours in all figures are drawn at 0.1 intervals. Regions where the correlation exceeds the

402 95% confidence level for significance are shaded in color (orange for positive and light blue

403 for negative).

404

405
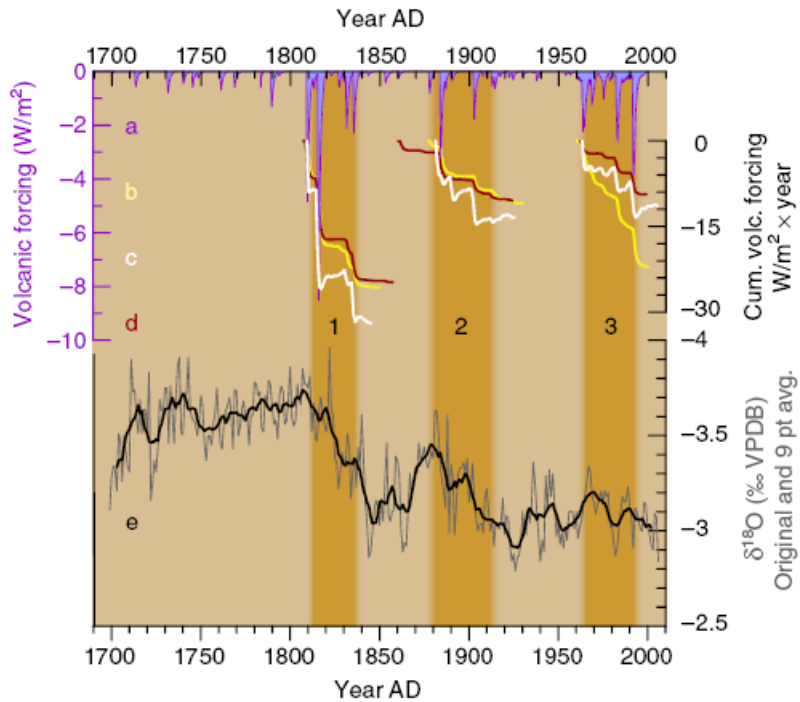
Figure 5: Persistent drying phases over Mesoamerica and volcanic forcing.(**a**) Volcanic

radiative forcing from 1700-2000 C. E.after[24]. Dark-brown boxes indicatevolcanic eruption

clusters noted in the text. (**b,c,d**)Different estimates of cumulative top-of-atmosphere radiative

flux anomalies from different climate simulations: BCM (Fig. 5b, yellow), CCSM4 (Fig. 5c,

white) and ECHAM5/MPIOM (Fig. 5d, brown). (**e**) Interpolated annual time series of

speleothemGU-Xi-1 δ^{18}O (grey line) with corresponding 11-year moving average values (thick

black line).

413
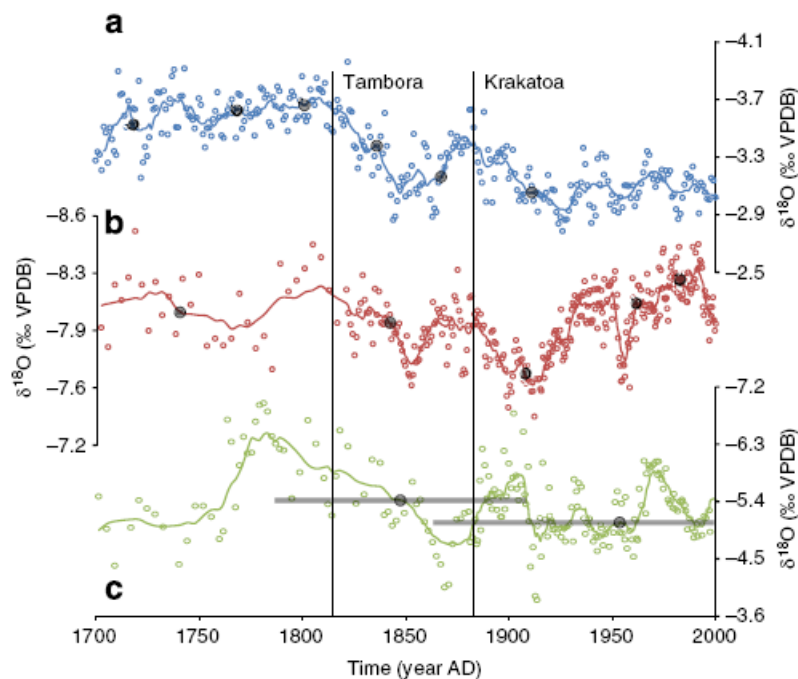
Figure 6: Comparison between stalagmite records from MesoAmerica. Top: GU-Xi-1 (this study); middle: southwestern Guerrero (Mexico)[13]; bottom: Yucatán peninsula (Mexico)[14].The difference in alignments of these records depends on their age models (note poor age control of theYucatánrecord[14]) sampling resolution and extent of local and cave environmental overprinting.
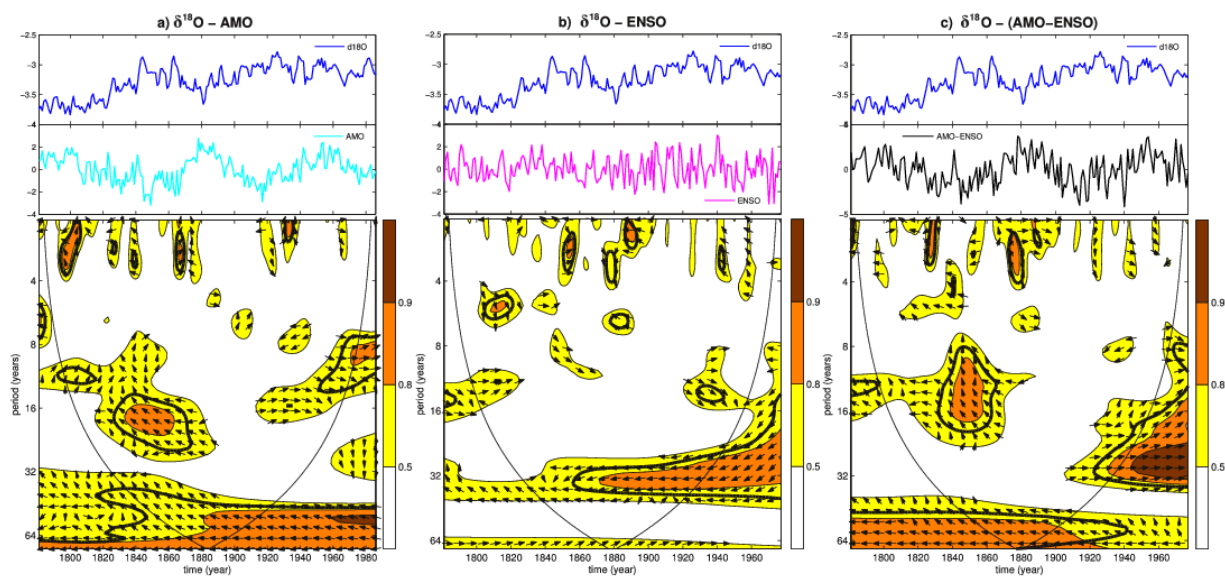
422 **Figure 7: Linkage between reconstructed Mesoamerican precipitation and dominant**

423 **modes of climate variability.** The different panels show wavelet coherences (power in color

424 shading) between the speleothem δ^{18}O and: **a**) the AMO reconstruction by[27], **b**) the integrated

425 ENSO/PDO reconstruction by[28], and **c**) the difference between the two. The time series are

426 shown in the top and middle panels (blue: δ^{18}O; turquoise: AMO; magenta: ENSO; black:

427 difference between AMO and ENSO). The arrows illustrate the phase relationship: rightward

428 (leftward) arrows indicate co-phase (anti-phase); northward and southward oriented arrows

429 indicate quadrature. Thick contour lines identify significant[58] coherence. The thin black lines

430 are the cone of influence, where edge effects occur.
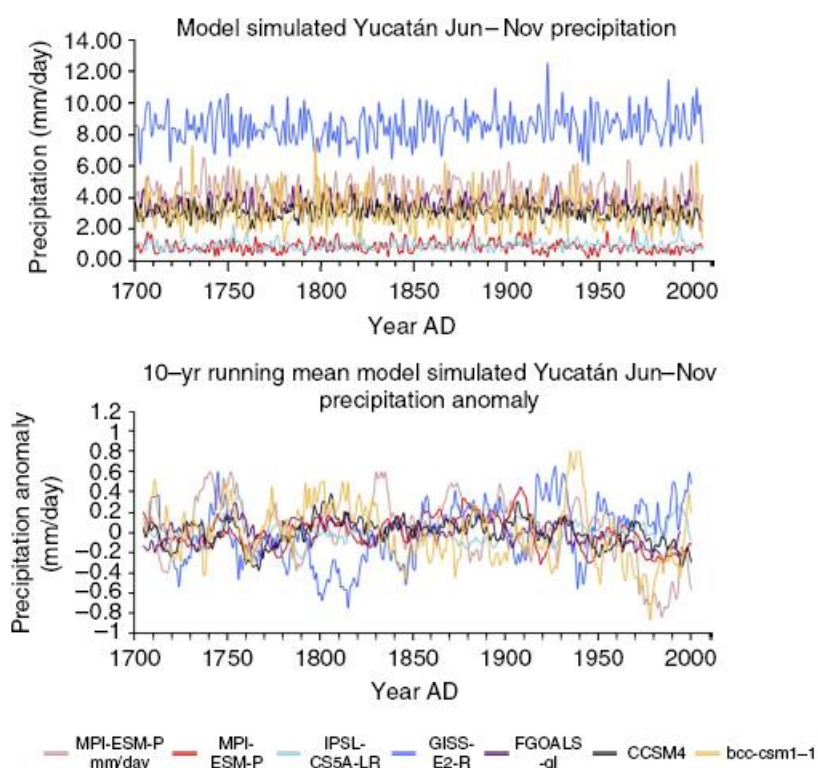
431

432 **Figure 8: June-November precipitation in Yucatán fromCMIP5 simulations covering the**

433 **period 1700 to 2005.a**) raw time series, **b**) 10-year running mean, where the climatological

434 mean has been subtracted.

435

436 **References**

1. Giannini, A., Kushnir, Y. & Cane, M. A. Interannual Variability of Caribbean Rainfall, ENSO, and the Atlantic Ocean. *J. Climate* **13,** 297–311 (2000).

2. Waliser, D. E. & Gautier, C. H. A satellite-derived climatology of the ITCZ. *J. Climate* **6**, 2162–2174 (1993).

3. Richey, J. N., Poore, R. Z., Flower, B. P., Quinn, T. M. & Hollander, D. J. Regionally coherent Little Ice Age cooling in the Atlantic Warm Pool. *Geophys. Res. Lett.* **36,** L21703 (2009).

4. Lachniet, M. S., Patterson, W. P., Burns, S., Asmerom, Y. &Polyak, V. Caribbean and Pacific moisture sources on the Isthmus of Panama revealed from stalagmite and surface water δ^{18}O gradients. *Geophys. Res. Lett.* **34,** L01708 (2007).

5. Seager, R. *et al.* Mexican drought: an observational modeling and tree ring study of variability and climate change. *Atmósfera***22,** 1–31 (2009).

6. Kushnir, Y., Seager, R., Ting, M., Naik, N. & Nakamura, J. Mechanisms of Tropical Atlantic SST Influence on North American Precipitation Variability. *J. Climate* **23,** 5610–5628 (2010).

7. Dai, A. &Wigley, T. M. L. Global patterns of ENSO-induced precipitation. *Geophys. Res. Lett.* **27,** 1283–1286 (2000).

8. Hurrell, J. W., *et al.* The North Atlantic Oscillation: Climatic significance and environmental impact. American Geophysical Union, *Geophysical Monograph* 134, 279 pp, (2002).

9. Miller, T. E. Geologic and Hydrologic Controls on Karst and Cave Development in Belize. *J. Cave Karst Stud.* **58**, 100–120 (1996).

10. Dansgaard, W. Stable isotopes in precipitation. *Tellus* **16**, 436–468 (1964).

11. Kennett, D. J. et al. Development and disintegration of Maya political systems in response to climate change. *Science* **338**, 788–791 (2012).

12. Lachniet, M. S. & Patterson, W. P. Oxygen isotope values of precipitation and surface waters in northern Central America (Belize and Guatemala) are dominated by temperature and amount effects. *Earth Planet. Sci. Lett.* **284**, 435–446 (2009).

13. Lachniet, M. S., Bernal, J. P., Asmerom, Y., Polyak, V. &Piperno, D. A 2400 yr Mesoamerican rainfall reconstruction links climate and cultural change. *Geology* **40,** 259-262 (2012).

468   14. Medina-Elizalde M, *et al.* High resolution climate record from the Yucatán Peninsula
469   spanning the Maya terminal classic period. *Earth Planet. Sci. Lett.* **298,** 255-262
470   (2010).

471   15. Webster, J. W. *et al.* Stalagmite evidence from Belize indicating significant droughts
472   at the time of Preclassic Abandonment, the Maya Hiatus, and the Classic Maya
473   collapse. *Palaeogeogr. Palaeoclimatol. Palaeoecol.* **250,** 1–17 (2007).

474   16. Bindoff, N.L. *et al* .Detection and Attribution of Climate Change: from Global to
475   Regional. In: Climate Change 2013: The Physical Science Basis. Contribution of
476   Working Group I to the Fifth Assessment Report of the Intergovernmental Panel on
477   Climate Change [Stocker, T.F., D. Qin, G.-K. Plattner, M. Tignor, S.K. Allen, J.
478   Boschung, A. Nauels, Y. Xia, V. Bex and P.M. Midgley (eds.)]. Cambridge
479   University Press, Cambridge, United Kingdom and New York, NY, USA (2013).

480   17. Ding, Y. *et al.* Ocean response to volcanic eruptions in Coupled Model
481   Intercomparison Project 5 (CMIP5) simulations. *J. Geophys. Res.* **119**, 5622-5637
482   (2014).

483   18. Santer B. D. *et. al.* Volcanic contribution to decadal changes in tropospheric
484   temperature. *Nature Geosci.* **7**, 185–189 (2014).

485   19. Rauscher, S. A., Giorgi, F., Diffenbaugh, N. S. & Seth, A. Extension and
486   Intensification of the Meso-American mid-summer drought in the twenty-first
487   century. *Clim. Dynam.* **31,** 551–571 (2008).

488   20. Ridley, H. E. *et al*. Aerosol forcing of the positionof the intertropical convergence
489   zone since AD 1550. *Nature Geosci.* **8** 195-200 (2014)

490   21. Anet, J. G. *et al.* Impact of solar versus volcanic activity variations on tropospheric
491   temperatures and precipitation during the Dalton Minimum. *Clim. Past,* **10**, 921–938,
492   (2014).

493   22. Schlesinger, M. E. An oscillation in the global climate system of period 65-70 years.
494   *Nature* **367**, 723–726 (1994).

495   23. Li, J. *et al.* El Niño modulations over the past seven centuries. *Nature Clim. Change*
496   **3**, 822–826 (2013).

497   24. Otterå, O. H., Bentsen, M., Drange, H. &Suo, L. External forcing as a metronome for
498   Atlantic multidecadal variability. *Nature Geosci.* **3**, 688–694 (2010).

499   25. Mignot, J., Khodri, M., Frankignoul, C. &Servonnat, J. Volcanic impact on the

500   Atlantic Ocean over the last millennium. *Clim. Past* **7,** 1439–1455 (2011).

501   26. Zanchettin, D. *et al.* Background conditions influence the decadal climate response to

502   strong volcanic eruptions. *J. Geophys. Res*. **118**, 1-17 (2013).

503   27. Svendsen, L., Hetzinger, S., Keenlyside, N. & Gao, Y. Marine-based multiproxy

504   reconstruction of Atlantic multidecadal variability. *Geophys. Res. Lett.* **41**,1295-1300,

505   (2014).

506   28. McGregor, S., Timmermann, A. &Timm, O. A unified proxy for ENSO and PDO

507   variability since 1650. *Clim. Past* **6**, 1-17 (2010).

508   29. Lehner, F., Raible, C. C. & Stocker, T. F. Testing the robustness of a precipitation

509   proxy-based North Atlantic Oscillation reconstruction. *Quat. Sc. Rev*. **45**, 85-94

510   (2012).

511   30. Stenchikov, G. *et al.* Arctic Oscillation response to volcanic eruptions in the IPCC

512   AR4 climate models. *J. Geophys. Res.* **111**, D07107 (2006).

513   31. Zanchettin, D. *et al.* Bi-decadal variability excited in the coupled ocean–atmosphere

514   system by strong tropical volcanic eruptions. *Clim. Dyn.* **39**, 1-2, 419-444 (2012)

515   32. Timmreck C. Modeling the climatic effects of large explosive volcanic eruptions.

516   *WIREs   Clim Change* **3**, 545–564 (2012).

517   33. Ault, T. R., Cole, J. E. & St. George, S. The amplitude of decadal to multidecadal

518   variability in precipitation simulated by state-of-the-art climate models. *Geophys.*

519   *Res. Lett*. **39**, L21705 (2012).

520   34. Zou,Y., Yu J.-Y., Lee T., Lu M.-M. & Kim S. T. CMIP5 model simulations of the

521   impacts of the two types of El Niño on the U.S. winter temperature, *J. Geophys. Res.*

522   *Atmos*. **119** (2014).

523   35. Kavvada, A., Ruiz-Barradas, A. & Nigam, S. AMO's structure and climate footprint

524   in observations and IPCC AR5 climate simulations. *Clim. Dyn*. **41**, 1345-1364

525   (2013).

526   36. Schmidt, G. A. *et al.*Using paleo-climate comparisons to constrain future projections

527   in CMIP5.*Clim. Past* **10**, 221–250 (2014).

528   37. Zorita, E. *et al.* Climate evolution in the last five centuries simulated by an

529   atmosphere-ocean model: global temperatures, the North Atlantic Oscillation and the

530   Late Maunder Minimum. *Meteorol. Z.* **13**, 271–289 (2004).

531   38. Ammann, C. M., Joos, F., Schimel, D. S., Otto-Bliesner, B. L. & Tomas, R. A. Solar

532   influence on climate during the past millennium: results from transient simulations

533   with the NCAR Climate System Model. *Proc. Natl. Acad. Sci. USA* **104,** 3713–3718

534   (2007).

535   39. Oman, L., Robock, A., Stenchikov, G. L. &Thordarson, T. High-latitude eruptions

536   cast shadow over the African monsoon and the flow of the Nile. *Geophys. Res. Lett.*

537   **33,** L18711 (2006).

538   40. Shen, C.-C. *et al.*Uranium and thorium isotopic and concentration measurements by

539   magnetic sector inductively coupled plasma mass spectrometry. *Chem. Geology* **185**,

540   165– 178 (2002).

541   41. Lauritzen S.-E. & Lundberg J. Calibration of the speleothem delta function: an

542   absolute temperature record for the Holocene in northern Norway. *The Holocene* **9**,

543   659–669 (1999).

544   42. Edwards R.L., Gallup C.D., & Cheng H. Uranium-series Dating of Marine and

545   Lacustrine Carbonates. *Rev. Mineral.Geochem.* **52**, 363-405 (2003).

546   43. Spötl, C. &Vennemann, T.W. Continuous-flow IRMS analysis of carbonate minerals.

547   *Rapid Comm. Mass Spectrom.* **17**, 1004-1006 (2003).

548   44. Scholz, D., Hoffmann, D.L. StalAge – An algorithm designed for construction of

549   speleothem age models. *Quat.Geochronol* .**6**, 369-382 (2011).

550   45. Breitenbach S. F. M. *et al.*Constructing Proxy Records from Age models (COPRA).

551   *Clim. Past*, **8**, 1765–1779 (2012).

552   46. Baker, A. *et al*. Testing theoretically predicted stalagmite growth rate with Recent

553   annually laminated samples: Implications for past stalagmite deposition,

554   *Geochim.Cosmochim.Acta* **62**: 393-404 (1998).

555   47. Fleitmann, D. &Spötl, C. Editorial: advances in speleothem research, PAGES news

556   **16**: 2 (2008).

557   48. Franke, H.W. The theory behind stalagmite shapes. *Studies in Speleology* **1**, 89-95

558   (1965).

559   49. Breitenbach S.F.M. &Bernasconi S.M. Carbon and oxygen isotope analysis of small

560   carbonate samples (20 to 100 μg) with a GasBench II preparation device. *Rapid*

561 *Comm. Mass Spectrom.* **25**, 1910–1914 (2011)

562 50. Smith, T.M., Reynolds, R. W., Peterson, T. C., &Lawrimore J. Improvements to

563 NOAA's Historical Merged Land-Ocean Surface Temperature Analysis (1880-2006).

564 *J. Clim.* **21**, 2283-2296 (2008).

565 51. Compo, G. P. *et al.* The Twentieth Century Reanalysis Project. *Quarterly. J. Roy.*

566 *Meteorol. Soc.* **137**, 1-28 (2011).

567 52. Jungclaus, J. H. *et al.* Climate and carbon-cycle variability over the last millennium.

568 *Clim. Past* **6**, 723-737 (2010).

569 53. Landrum, L. *et al.* Last Millennium Climate and Its Variability in CCSM4. *J. Clim.*

570 **26**, 1085- 1111 (2012).

571 54. Crowley, T. *et al.* Volcanism and the Little Ice Age. *PAGES Newsletter* **16**, 22–23

572 (2008).

573 55. Crowley, T. J. *et al*. Modeling ocean heat content changes during the last millennium.

574 *Geophys. Res. Lett.* **30**, 1932 (2003)

575 56. Gao, C., Robock A. & Ammann C. Volcanic forcing of climate over the last 1500

576 years: An improved ice core–based index for climate models. *J. Geophys. Res.* **113**,

577 (2008).

578 57. Dawdy, D.R. &Matalas, N.C. Statistical and probability analysis of hydrologic data,

579 part III: Analysis of variance, covariance and time series, in VenTe Chow, ed.

580 *Handbook of applied hydrology, a compendium of water-resources technology*: New

581 York, McGraw-Hill Book Company, p. 8.68-8.90 (1964)

582 58. Grinsted, A Moore J. C. & Jevrejeva S. Application of the cross wavelet transform

583 and wavelet coherence to geophysical time series. *Nonlin. Proc. Geophys.***11**, 561–

584 566 (2004).

585 59. Torrence, C. & Compo G. P. A practical guide to wavelet analysis. *Bull. Am. Meteor.*

586 *Soc.* **79**, 61-78 (1998).

587

588